Asymmetrical effects of mesophyll conductance on fundamental photosynthetic parameters and their relationships estimated from leaf gas exchange measurements

Citation	Sun, Y., Gu, L., Dickinson, R. E., Pallardy, S. G., Baker, J., Cao, Y., ... & Winter, K. (2014). Asymmetrical effects of mesophyll conductance on fundamental photosynthetic parameters and their relationships estimated from leaf gas exchange measurements. Plant, Cell & Environment, 37(4), 978-994. doi:10.1111/pce.12213
DOI	10.1111/pce.12213
Publisher	John Wiley & Sons Ltd.
Version	Version of Record
Terms of Use	http://cdss.library.oregonstate.edu/sa-termsofuse

Plant, Cell & Environment

Plant, Cell and Environment (2014) **37**, 978–994 doi: 10.1111/pce.12213

Original Article

Asymmetrical effects of mesophyll conductance on fundamental photosynthetic parameters and their relationships estimated from leaf gas exchange measurements

Ying Sun[1], Lianhong Gu[2], Robert E. Dickinson[1], Stephen G. Pallardy[3], John Baker[4], Yonghui Cao[5], Fábio Murilo DaMatta[6], Xuejun Dong[7], David Ellsworth[8], Davina Van Goethem[9], Anna M. Jensen[2], Beverly E. Law[10], Rodolfo Loos[11], Samuel C. Vitor Martins[6], Richard J. Norby[2], Jeffrey Warren[2], David Weston[12] & Klaus Winter[13]

[1]Department of Geological Sciences, University of Texas at Austin, 1 University Station #C9000, Austin, TX 78712, USA, [2]Environmental Sciences Division, Oak Ridge National Laboratory, Oak Ridge, TN 37831, USA, [3]Department of Forestry, University of Missouri, Columbia, MO 65211, USA, [4]USDA Soil & Water Management Unit & Department of Soil, Water & Climate, University of Minnesota, 1991 Upper Buford Circle, St. Paul, MN 55108, USA, [5]Research Institute of Subtropical Forestry, Chinese Academy of Forestry, Fuyang, Zhejiang, China, [6]Departamento de Biologia Vegetal, Universidade Federal de Viçosa, 36570-000 Viçosa, MG, Brazil, [7]Central Grasslands Research Extension Center, North Dakota State University, Streeter, ND 58483, USA, [8]Hawkesbury Institute for the Environment, University of Western Sydney, Locked Bag 1797, Penrith, NSW 2751, Australia, [9]Department of Bio-science Engineering, University of Antwerp, Groenenborgerlaan 171, Antwerp 2020, Belgium, [10]College of Forestry, Oregon State University, Corvallis, OR 97331, USA, [11]Technology Center, Fibria Celulose S.A, Rod. Aracruz-Barra do Riacho – km 25, Aracruz 29197900, Brazil, [12]Biosciences Division, Oak Ridge National Laboratory, Oak Ridge, TN 37831, USA and [13]Smithsonian Tropical Research Institute, PO Box 0843-03092, Balboa, Ancon, Republic of Panama

ABSTRACT

Worldwide measurements of nearly 130 C_3 species covering all major plant functional types are analysed in conjunction with model simulations to determine the effects of mesophyll conductance (g_m) on photosynthetic parameters and their relationships estimated from A/C_i curves. We find that an assumption of infinite g_m results in up to 75% underestimation for maximum carboxylation rate V_{cmax}, 60% for maximum electron transport rate J_{max}, and 40% for triose phosphate utilization rate T_u. V_{cmax} is most sensitive, J_{max} is less sensitive, and T_u has the least sensitivity to the variation of g_m. Because of this asymmetrical effect of g_m, the ratios of J_{max} to V_{cmax}, T_u to V_{cmax} and T_u to J_{max} are all overestimated. An infinite g_m assumption also limits the freedom of variation of estimated parameters and artificially constrains parameter relationships to stronger shapes. These findings suggest the importance of quantifying g_m for understanding *in situ* photosynthetic machinery functioning. We show that a nonzero resistance to CO_2 movement in chloroplasts has small effects on estimated parameters. A non-linear function with g_m as input is developed to convert the parameters estimated under an assumption of infinite g_m to proper values. This function will facilitate g_m representation in global carbon cycle models.

Key-words: A/C_i curves; carbon cycle model; leaf photosynthesis; LeafWeb; parameter estimation.

Correspondence: L. Gu. E-mail: lianhong-gu@ornl.gov

INTRODUCTION

Leaf gas exchange measurements that relate CO_2 assimilation (A) to changes of CO_2 partial pressure in leaf substomatal cavities (C_i), that is the so-called A/C_i curves, provide crucial information on photosynthetic processes (Wullschleger 1993; Long *et al*. 1996; von Caemmerer 2000; Long & Bernacchi 2003). Key biochemical parameters of photosynthesis can be estimated by fitting A/C_i curves with the mechanistic Farquhar–von Caemmerer–Berry (FvCB) model (Farquhar *et al*. 1980; Farquhar & von Caemmerer 1982) as modified by Sharkey (1985) and von Caemmerer (2000). Parameter estimation approaches with the FvCB model have been discussed previously (e.g. Ethier & Livingston 2004; Manter & Kerrigan 2004; Ethier *et al*. 2006; Dubois *et al*. 2007; Sharkey *et al*. 2007; Miao *et al*. 2009; Yin *et al*. 2009; Gu *et al*. 2010). The estimated parameters are then related to physiological or environmental variables such as leaf morphology and nutrient contents, canopy environmental gradients, and soil conditions to characterize the underlying eco-physiological processes (e.g. Niinemets *et al*. 2001; Warren *et al*. 2003; Ellsworth *et al*. 2004;

Hikosaka 2005; Onoda *et al*. 2005a,b; Busch *et al*. 2013). They are also employed in ecosystem and land surface models to simulate responses of terrestrial carbon and water cycles to environmental variations at various spatial and temporal scales (e.g. Schwarz *et al*. 2004; Kattge *et al*. 2009; Bonan *et al*. 2011).

The theoretical framework of the FvCB model requires the CO_2 partial pressure at the carboxylation site, that is the chloroplast (C_c), not C_i (Evans *et al*. 1986). Most previous studies, including those of the global carbon cycle, however, have ignored the internal movement of CO_2 from leaf substomatal cavity to chloroplast and applied the FvCB model directly to C_i, a practice that compromises the theoretical integrity of the FvCB model. The integrity of the model can be maintained if it is extended to explicitly consider this internal movement process from leaf substomatal cavity to chloroplast, which can be characterized by a parameter referred to as mesophyll conductance (g_m) (Ethier & Livingston 2004; Niinemets *et al*. 2009b; Gu *et al*. 2010). The extended FvCB model can then be fitted to the A/C_i curves to estimate biochemical parameters, together with g_m. In this way, C_c, instead of C_i, is directly applied to the FvCB model, as if the A/C_c curves were being fitted, and the parameters obtained can be appropriately termed A/C_c-based parameters to differentiate them from the conventional A/C_i-based parameters.

The mesophyll conductance g_m controls the CO_2 drawdown from C_i to C_c (Evans *et al*. 1986; Niinemets *et al*. 2009b,c). This drawdown vanishes only if g_m is infinitely large. However, plant species have a finite value of g_m, which can significantly affect photosynthetic rates (Evans *et al*. 1986; Ethier & Livingston 2004; Ethier *et al*. 2006; Flexas *et al*. 2008; Warren 2008; Niinemets *et al*. 2009c). Without explicitly considering g_m, the A/C_i-based estimates of key biochemical parameters as well as the relationships among them may be biased (Ethier & Livingston 2004; Niinemets *et al*. 2009a,b,c). Furthermore, the use of biased A/C_i-based values of these parameters to predict photosynthesis under field conditions may either overestimate or underestimate actual photosynthesis, depending on the magnitude of g_m and environmental stresses (Niinemets *et al*. 2009a,b,c).

A vast amount of A/C_i curves have already been analysed without explicit consideration of g_m. Photosynthetic parameters derived from such analyses have been widely used in process-based studies of plant physiology, ecology and global change biology as well as in local, regional and global modelling research (e.g. Wullschleger 1993; Onoda *et al*. 2005a,b; Kattge *et al*. 2009; Bonan *et al*. 2011). Evaluation of the reliability of these studies requires a clear understanding of the effects of g_m on photosynthetic parameter estimation across species and climates. Previously published papers that included raw A/C_i data would allow a refitting to estimate the A/C_c-based parameters with explicit consideration of g_m using approaches such as that of Ethier & Livingston (2004) and Gu *et al*. (2010). Unfortunately, most papers did not include raw data, making refitting infeasible. In order to make use of the rich resources represented in the past literature of A/C_i curve analyses and to facilitate the transition from an infinite g_m-based to a more realistic finite g_m-based modelling of photosynthesis, it is necessary to understand how g_m affects the values of key photosynthetic parameters as well as the functional relationships among them in wide ranges of species and climates.

Mesophyll conductance g_m varies widely across leaf traits and plant functional types (Syvertsen *et al*. 1995; Flexas *et al*. 2008; Niinemets *et al*. 2009c), light gradients inside plant canopies (Hanba *et al*. 2002; Piel *et al*. 2002; Laisk *et al*. 2005; Terashima *et al*. 2006; Warren *et al*. 2007; Montpied *et al*. 2009; Han *et al*. 2010) and with environmental stress factors (Chazen & Neumann 1994; Miyazawa *et al*. 2008). For a small set of samples with very limited variations in g_m and photosynthetic capacities, a simple linear relationship may be used to convert the biased A/C_i-based parameters to the corresponding unbiased A/C_c-based parameters (Zeng *et al*. 2010). But it is unlikely that a universal correction factor exists across species and environmental gradients given the large variations of g_m (Niinemets *et al*. 2009c). Schemes that can achieve this conversion will at least have to use g_m as input. Such schemes will be very useful in facilitating the transition from A/C_i-based to A/C_c-based parameter estimation and in large-scale terrestrial carbon cycle modelling.

This study presents a systematic evaluation of the effects of g_m on the values and relationships of photosynthetic parameters V_{cmax} (the maximum carboxylation rate), J_{max} (the maximum electron transport rate) and T_u (the triose phosphate utilization rate) estimated through A/C_i analyses. An emphasis is placed on the functional relationships among these parameters because accurate quantification of these relationships will clarify gas exchange-based analyses of the photosynthetic process and because such relationships are frequently used in scaling up photosynthesis from leaf to canopy to globe (e.g. Bonan *et al*. 2011). We aimed to develop practical solutions to enable large-scale carbon cycle models to represent the internal CO_2 transfer process explicitly. We use worldwide measurements of leaf gas exchange of nearly 130 species from all major plant functional types and climates to identify general patterns. The data collection was made possible by a free web-based tool called LeafWeb (http://leafweb.ornl.gov), which conducts automated A/C_i and A/C_c curve analyses and also provides an estimate of g_m. The findings from these field measurements are further corroborated with analyses based on systematically simulated A/C_i curves. This study attempts to address the following questions:

1. For a given value of g_m, how do the 'apparent', A/C_i –based V_{cmax}, J_{max} and T_u parameters (denoted as $V_{cmax,i}$, $J_{max,i}$ and $T_{u,i}$, respectively) vary with the 'true', A/C_c-based V_{cmax}, J_{max} and T_u parameters (denoted as $V_{cmax,c}$, $J_{max,c}$ and $T_{u,c}$, respectively)?
2. Are different A/C_i-based parameters equally sensitive to the variation of g_m?
3. For a given set of the A/C_c-based parameters, how do the A/C_i-based parameters vary with g_m?
4. How do the relationships among $V_{cmax,c}$, $J_{max,c}$ and $T_{u,c}$ differ from those among $V_{cmax,i}$, $J_{max,i}$ and $T_{u,i}$?

5 Is there a mathematical function that can be used to accurately convert the A/C_i-based parameters to the A/C_c –based parameters for a wide range of photosynthetic capacities, g_m values and environmental factors?

To eliminate factors that may bias the interpretations for the questions mentioned earlier, we will first examine consequences of potential nonzero resistance (r_{ch}) to CO_2 movement across chloroplast envelopes and stroma in the framework of Tholen *et al*. (2012). We will also clarify whether different values of Rubisco kinetic parameters, that is K_c, K_o and the chloroplastic CO_2 compensation point Γ^* can be used to compensate for the omission of g_m in estimating V_{cmax}, J_{max} and T_u. These two efforts establish the rationale for our approach to addressing the five main questions listed earlier.

METHODS

General considerations

Both actual and simulated A/C_i curves are used in this study. The simulated A/C_i curves, although artificial, allow the true values of parameters of interest to be controlled and thus make it possible to answer some questions with absolute certainty (e.g. for a given value of the true, A/C_c-based parameter, how does the apparent, A/C_i-based parameter vary with g_m?). The actual and simulated A/C_i curves are analysed with and without explicit consideration of g_m in the same way, providing an independent check on findings obtained from actual A/C_i curves.

The term mesophyll conductance as used in this study is defined technically as the ratio of net photosynthetic rate (A) to the difference between C_i and C_c, that is, $g_m = A/(C_i - C_c)$, consistent with Fick's law of diffusion and definitions of other conductance terms such as stomatal and boundary-layer conductance. The same phrase has also been used to describe the initial slope of A/C_i curves in some previous papers (e.g. Sinclair *et al*. 1977) as well as in current manuals of some instruments of leaf gas exchange measurements (e.g. LI-6400/LI-6400XT Instruction Manual, Version 6, http://www.licor.com/env/products/photosynthesis/manuals.html). This second use of the same term mesophyll conductance is confusing. We suggest that the concept of mesophyll conductance be used exclusively in the framework of Fick's law of diffusion.

Although using a single parameter, that is mesophyll conductance, to characterize the diffusion and transport of CO_2 inside leaves has been surprisingly successful (Sharkey 2012), it has limitations (Tholen & Zhu 2011; Tholen *et al*. 2012). It simplifies the three-dimensional mesophyll architecture to a one-dimensional tubing with all Rubisco at one end and all intercellular air space at the other. Furthermore, to treat g_m as a constant parameter rather than a variable, one has to assume that the resistance to CO_2 movement caused by the chloroplast envelope and stroma (r_{ch}) is much smaller than that by cell walls and plasmalemma (r_{wp}); otherwise, g_m varies with C_i and the ratio of the respiratory rate (photorespiration + day respiration) to the net photosynthetic rate and correlates with stomatal conductance (Tholen *et al*. 2012). Fortunately, such dependence is only strong at low C_i while at high C_i, g_m is almost constant (Gu & Sun 2013); also a nonzero r_{ch} mostly affects the estimation of day respiration R_d and Γ^*, and its effect on estimation of V_{cmax} appears to be negligible (Tholen *et al*. 2012). Ideally it would be better to estimate r_{ch} and r_{wp} instead of g_m. However, the FvCB model is already overparameterized with respect to typical leaf gas exchange measurements (Gu *et al*. 2010) and adding one more parameter to the equation may adversely affect the estimation of other parameters. Nevertheless, to ensure the broad validity of results from this study, we use systematic simulations to evaluate the impact of a nonzero r_{ch} on estimated V_{cmax}, J_{max} and T_u for a range of r_{ch} and r_{wp} values.

Some researchers have used different Rubisco Michaelis–Menten parameters (K_c and K_o) and Γ^* depending on whether g_m is assumed infinite or finite (von Caemmerer *et al*. 1994). Thus, we use simulations to investigate if adjustments to K_c, K_o and Γ^* can be used to obtain reliable estimates of $V_{cmax,c}$, $J_{max,c}$ and $T_{u,c}$ even when g_m is assumed infinite. Throughout this paper, Γ^* strictly represents the chloroplastic CO_2 compensation point, that is, the CO_2 compensation point in the absence of day respiration R_d, and is different from C_i^*, the CO_2 compensation point in the presence of R_d.

A/C_i curve measurements

The A/C_i curve measurements used in this study were from about 130 C_3 plant species in Australia, Brazil, China, France, Ireland, Panama and the United States. In total, more than 1000 measured curves were actually used in the analysis. Although LeafWeb had accumulated more curves, we excluded those that did not yield adequate fitting. The criteria used to select reliable measured curves were detailed in Gu *et al*. (2010). The Appendix I lists the species, which include grasses, herbs, crops, shrubs and trees (deciduous and evergreen broadleaf and conifers), and their locations. All A/C_i curves were measured with Li-6400 portable photosynthetic systems (LiCor Environmental Sciences, Lincoln, NE, USA). Measurements followed standard protocols (Long *et al*. 1996; Long & Bernacchi 2003). Targeted light response curves were used to ensure that light intensities were set at saturating levels appropriate to species and their growth environments. Leaf temperatures were generally controlled to be within 3 °C of the corresponding ambient air temperatures while within a curve, variations in leaf temperatures were generally less than 2 °C. The average leaf temperature across the curves was 26(±5) °C and PAR 1255 (±323) μmol m^{-2} s^{-1}. Relative humidity was set generally between 55 and 75%. Stomatal ratios were set based on researchers' knowledge of the relative distribution of stomata on the two sides of the leaf. Flow rates were mostly between 300 and 500 μmol s^{-1}. CO_2 injectors were used to control reference CO_2 in typical sequences starting from a value close to ambient (e.g. 400 ppm), decreasing to a minimum value (e.g. 50 ppm), returning to the starting value (as a check point), and then increasing to a maximum value (e.g. 1500 ppm). Each curve contained at least 10 points. The reference and sample chambers were matched manually or automatically as needed. Ample time

was allowed for leaves to adapt to chamber environment and to changes in CO_2 concentrations. For coniferous species, variables and parameters were based on projected leaf areas.

A/C$_i$ curve simulations

We simulated A/C_i curves with the FvCB model extended with the g_m representation, using procedures adopted from Gu *et al*. (2010). The values of key photosynthetic parameters and sampling points were all selected randomly except for certain constraints that were set to either satisfy the conditions required by the FvCB model or to answer particular questions. Each simulated A/C_i curve contained 15 points and each point in a curve was limited either by Rubisco, or by ribulose-1,5-bisphosphate (RuBP) regeneration, or by the triose phosphate utilization (TPU). For a curve to be valid, all three limitation states must be present and in an orderly fashion with at least 3 points for Rubisco, 3 points for RuBP regeneration, 2 points for TPU (Gu *et al*. 2010). The minimum number of requirement ensures that no over-fitting occurs and the actual parameters used in generating the A/C_i curves can be properly retrieved in fitting. The C_i values of the 15 points of a simulated A/C_i curve were, respectively, 5, 10, 15, 20, 25, 30, 35, 40, 45, 50, 55, 60, 70, 80 and 90 Pa, all multiplied by a factor that randomly varied from 0.5 to 1.5. This scheme of generating C_i values was designed such that the obtained 15 C_i values were distributed along the C_i axis in a way that resembles typical A/C_i curve measurements. The randomness in the multiplying factor ensures that the C_i values varied from curve to curve. We experimented with different sequences of C_i values and did not find any qualitative difference in terms of the final results reported in this study, indicating the random process is adequate in generating representative C_i values for simulated A/C_i curves.

Different A/C_i curves were simulated by varying the values of $V_{cmax,c}$, $J_{max,c}$, $T_{u,c}$ and g_m. These parameters were varied either systematically or randomly, depending on what specific questions were addressed. An A/C_i curve cannot be produced by any arbitrary combination of $V_{cmax,c}$, $J_{max,c}$ and $T_{u,c}$. Gu *et al*. (2010) showed that the FvCB formulation of photosynthesis requires the following inequality to hold for all three limitation states to occur in the same A/C_i curve:

$$4V_{cmax,c} > J > 12T_{u,c} \quad (1)$$

Here, J is the actual electron transport rate and is a function of $J_{max,c}$ and the incident light level on the leaf. The inequality in Eqn 1 is a necessary condition for the orderly occurrence of the three limitation states along the C_i axis of an A/C_i curve. Thus, we imposed this condition when the parameter sets were selected.

To determine how $V_{cmax,i}$ changes with $V_{cmax,c}$ for a given g_m, or with g_m for a given $V_{cmax,c}$, $V_{cmax,c}$ and g_m were varied in prescribed intervals with nested loops (the variation in one parameter occurs within the variation of the other) while the values of $J_{max,c}$ and $T_{u,c}$ were randomly generated. If the randomly generated values of $J_{max,c}$ and $T_{u,c}$ did not satisfy the inequality in Eqn 1 or if the minimum number requirements for Rubisco-, RuBP regeneration- and TPU-limited states were not met, these values were discarded and new values of $J_{max,c}$ and $T_{u,c}$ were randomly generated (but the same $V_{cmax,c}$ and g_m values were kept). To determine how $J_{max,i}$ changes with $J_{max,c}$ for a given g_m, or with g_m for a given $J_{max,c}$, $J_{max,c}$ and g_m were varied in prescribed intervals with nested loops while $V_{cmax,c}$ and $T_{u,c}$ were varied randomly. If the randomly generated values of $V_{cmax,c}$ and $T_{u,c}$ did not satisfy the inequality in Eqn 1 or if the minimum number requirements were not met, these values were discarded and new values of $V_{cmax,c}$ and $T_{u,c}$ were randomly generated (but the same $J_{max,c}$ and g_m values were kept). A similar scheme was used to generate A/C_i curves for determining how $T_{u,i}$ changes with $T_{u,c}$ for a given g_m, or with g_m for a given $T_{u,c}$. An additional 5000 A/C_i curves were simulated by varying all parameters randomly to increase the variability of parameter values of the simulated A/C_i curves for parameter relationship analyses. During all these simulations, light was set at 1000 μmol m^{-2} s^{-1} (a typical value in A/C_i curve measurements), R_d at $0.015 \times V_{cmax,c}$ (e.g. Niinemets *et al*. 1998; Bonan *et al*. 2011; thus R_d was not an independent parameter in any of the simulations) and leaf temperature at 25 °C. K_c, K_o and Γ^* were fixed for all simulated A/C_i curves at the values given in Table 1 of Sharkey *et al*. (2007).

The above simulations effectively assume $r_{ch} = 0$. To evaluate the potential consequences of a nonzero r_{ch} within the mesophyll diffusion framework of Tholen *et al*. (2012), we also generated a separate set of simulated A/C_i curves with $r_{ch} > 0$. These nonzero-r_{ch} curves were then analysed as if $r_{ch} = 0$. The estimated $V_{cmax,c}$, $J_{max,c}$ and $T_{u,c}$ were then compared with the corresponding true values. The nonzero-r_{ch} curves were generated as follows (Gu & Sun 2013). For a given set of photosynthetic parameters (i.e. $V_{cmax,c}$, $J_{max,c}$, $T_{u,c}$, R_d, Γ^*, r_{wp}, r_{ch}), first we computed A and the carboxylation rate V_c for a given value of C_c with the model of Farquhar *et al*. (1980) as presented in Gu *et al*. (2010). Then we computed the CO_2 partial pressure in cytosol (C_y) with the following equation (Tholen *et al*. 2012; Gu & Sun 2013):

$$C_y = C_c + r_{ch}V_c \quad (2)$$

Next, we calculated C_i as follows:

$$C_i = C_y + r_{wp}A \quad (3)$$

Table 1. The values of empirical constants for the function (Eqn 4) that relates the A/C_i to A/C_c-based parameters

	a	*b*	*c*	*d*	R^2	RMS (μmol m^{-2} s^{-1})
$V_{cmax,c}$	0.1164	1.2643	0.6429	0.9431	0.83	18.0437
$J_{max,c}$	0.0084	0.7552	0.6230	–0.1166	0.97	7.5290
$T_{u,c}$	0.1249	1.8059	0.2525	1.5905	0.99	0.3597

RMS, root mean square error.

A full nonzero-r_{ch} A/C_i curve was generated by repeating the procedure mentioned earlier with different C_c value. This procedure is different from that used to generate zero-r_{ch} A/C_i curves because the equations for expressing A explicitly as a function of C_i are already available for zero-r_{ch} curves (Ethier & Livingston 2004; Gu *et al*. 2010) while the derivation of such equatuions for nonzero-r_{ch} curves is beyond the scope of the current study.

A/C$_i$ curve fitting

The measured and simulated A/C_i curves were analysed with the approach of Gu *et al*. (2010) which is an extension to that of Ethier & Livingston (2004) and is the same as that used in LeafWeb. Gu *et al*.'s approach avoids arbitrarily assigning transitional thresholds by allowing any point of a given A/C_i curve to be in any of the three limitation states and then enumerating all possible scenarios (limitation state combinations). The scheme of enumeration considers that instead of occurring in a random sequence, the three limitation states must follow certain pattern along the C_i (C_c) axis in order to be consistent with the FvCB model, that is the C_i (C_c) values for the Rubisco-limited state should be smaller than those of the RuBP regeneration-limited state, which in turn should be smaller than for the TPU-limited points. Each scenario is then fit separately with the limitation state of each point fixed to ensure a smooth cost function for the change-point FvCB model. During this process, the so-called inadmissible fits are detected and corrected via a penalization strategy. The best fit among all scenarios is selected. Thus the approach of Gu *et al*. (2010) has two nested optimizations – the optimization for limitation state combination and the optimization for parameters from the optimized limitation state combination.

The fitting procedures described earlier are applied twice for each curve. In the first fitting, g_m is assumed infinite and the A/C_i-based parameters are estimated; in the second fitting, g_m is estimated together with other A/C_c-based parameters. Parameters are standardized to a reference temperature of 25 °C. The kinetic constants and coefficients in the temperature response functions, which are taken from Table 1 of Sharkey *et al*. (2007), are kept the same for all fittings except for the simulations that are designed to determine whether different values of K_c, K_o and Γ^* can be used to compensate for the impact of assuming an infinite g_m to obtain reliable estimates of $V_{cmax,c}$, $J_{max,c}$ and $T_{u,c}$. In these simulations, the composite parameter K_{co} [$= K_c(1 + O/K_o)$, Gu *et al*. 2010] and Γ^* are optimized together with V_{cmax}, J_{max} and T_u with an assumption of an infinite g_m.

RESULTS

What are the potential effects of a nonzero r_{ch} and can different K_c, K_o and Γ^* be used to compensate for the effects of g_m?

Figure 1 shows simulated effects of a nonzero r_{ch} on estimated photosynthetic parameters. In these simulations, three different values of r_{wp} were used (0.5, 1.0 and 2.0 Pa m^2 s

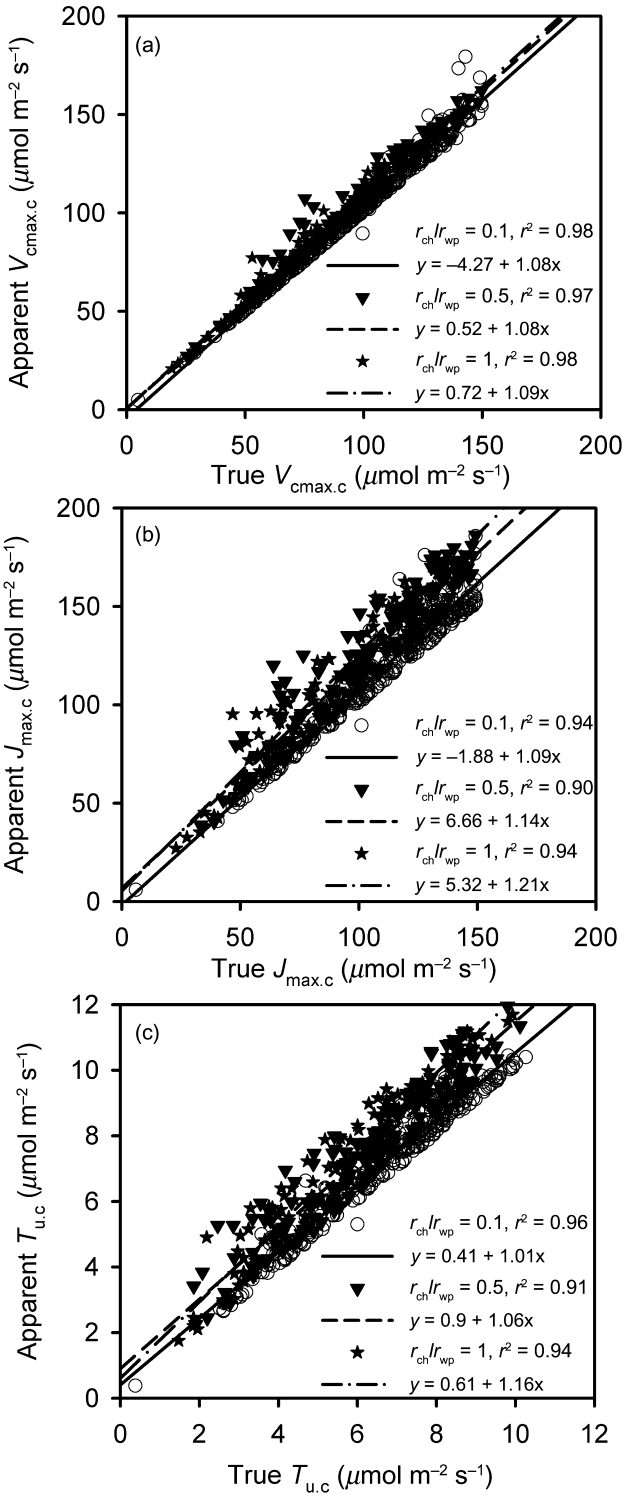

Figure 1. The relationships between apparent and true parameters of $V_{cmax,c}$ (a), $J_{max,c}$ (b), and $T_{u,c}$ (c) for simulated A/C_i curves with different ratios of r_{ch} to r_{wp}. The estimated parameters are obtained by assuming $r_{ch} = 0$ even when the true r_{ch} is not zero.

μmol^{-1}) and for each r_{wp}, three r_{ch}/r_{wp} ratios (0.1, 0.5 and 1.0) were used. For each combination of r_{ch} and r_{wp}, $V_{cmax,c}$, $J_{max,c}$, $T_{u,c}$ were randomly selected. We compare the estimates of $V_{cmax,c}$ (Fig. 1a), $J_{max,c}$ (Fig. 1b) and $T_{u,c}$ (Fig. 1c) when a zero r_{ch} is assumed (y axis) versus their corresponding true values, that is when the true r_{ch} is not zero (x axis). We find that different r_{wp} values result in similar patterns and therefore are grouped together, but different r_{ch}/r_{wp} ratios result in slightly different patterns and therefore are separated. Assuming a zero r_{ch} when the true r_{ch} is not zero produces less than 10% error for the estimated $V_{cmax,c}$ (Fig. 1a), regardless the ratio of r_{ch}/r_{wp}, which is consistent with the finding of Tholen *et al.* (2012). For $J_{max,c}$ ($T_{u,c}$), the error is less than 15% (10%) when the r_{ch}/r_{wp} ratio is less than 0.5. Only when r_{ch} has the same magnitude as r_{wp} is the error for the two parameters larger than 15%.

Thus a nonzero r_{ch} can potentially cause some uncertainties in the estimation of $V_{cmax,c}$, $J_{max,c}$ and $T_{u,c}$. At present, there is a lack of data on the magnitude of r_{ch} relative to r_{wp} for any plant species. However, it has been widely observed that chloroplasts are often positioned close to the cell walls and plasmalemma while the mitochondria are located further inside the cells (Nobel 2009). With this geometry, CO_2 evolved from the mitochondria must diffuse through the chloroplasts to reach the intercellular air spaces. From a modelling perspective, this is equivalent to as if the mitochondria and Rubisco shared the same compartment and r_{ch} was effectively zero. Thus for the purpose of this present study, it is probably justifiable to assume a zero r_{ch}. As shown later, our results based on measurements are consistent with corresponding analyses based on simulations, which supports this assumption.

We further examine, with simulations, whether different K_c, K_o and Γ^* can be used to compensate for the effects of g_m. The simulations either randomly selected g_m from the range of $1/g_m$ between 0 and 5 Pa m^2 s μmol^{-1} or used fixed values within this range. We present results from randomly selected g_m in Fig. 2; results from fixed g_m are similar. Figure 2 shows that reliable estimates of $V_{cmax,c}$ (Fig. 2a) and $J_{max,c}$ (Fig. 2b) cannot be achieved by optimizing parameters of K_c and K_o (through K_{co}) and Γ^* but ignoring g_m. The estimates of V_{cmax} and J_{max} corresponding to the optimized K_{co} and Γ^* are generally much smaller than their corresponding true values. However, the impact on the estimate of $T_{u,c}$ is negligible (Fig. 2c).

In the following presentation of results, we ignore the potential impacts of a nonzero r_{ch} and use consistent, A/C_c-based parameters of K_c, K_o and Γ^* for the comparisons between parameter estimations with and without g_m considerations. However, we acknowledge that effects of a nonzero r_{ch} require further studies.

Results based on actual leaf gas exchange measurements

Figures 3–5 present results on parameters inferred from measured A/C_i curves across plant functional types and climates. We pooled the data together because we found that

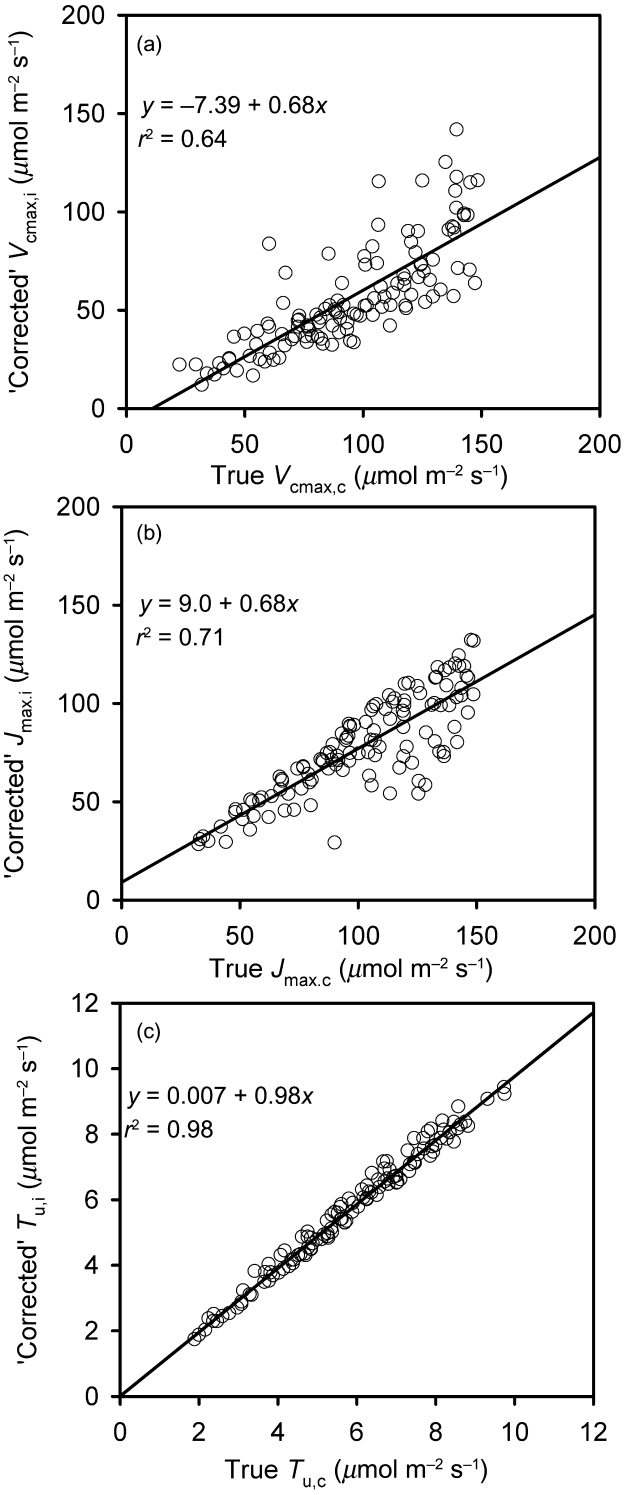

Figure 2. The relationships between estimated ('corrected') $V_{cmax,i}$ and true $V_{cmax,c}$ (a), estimated $J_{max,i}$ and true $J_{max,c}$ (b), estimated $T_{u,i}$ and true $T_{u,c}$ (c) for simulated A/C_i curves with randomly varying parameters. The estimation of $V_{cmax,i}$, $J_{max,i}$ and $T_{u,i}$ is conducted with simultaneous optimization of K_{co} and Γ^* while assuming an infinite g_m when the true g_m is finite.

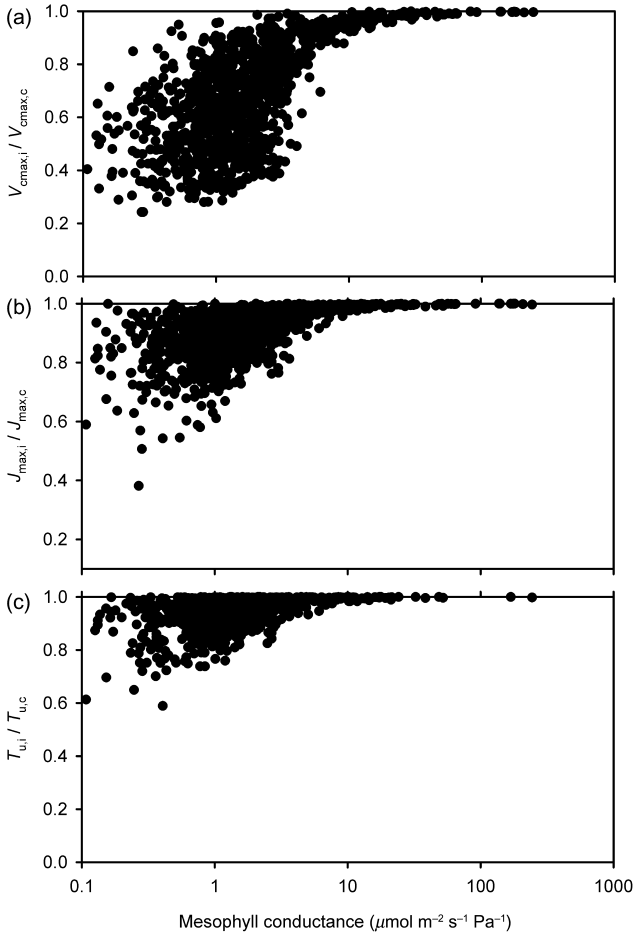

Figure 3. The ratios of the A/C_i-based to corresponding A/C_c-based parameters as a function of mesophyll conductance. The A/C_i-based parameters are estimated by assuming infinite mesophyll conductance while the A/C_c-based parameters are estimated together with mesophyll conductance. Mesophyll conductance is expressed in logarithmic scale. (a) the ratio of A/C_i-based V_{cmax} ($V_{cmax,i}$) to A/C_c-based V_{cmax} ($V_{cmax,c}$); (b) the ratio of A/C_i-based J_{max} ($J_{max,i}$) to A/C_c-based J_{max} ($J_{max,c}$); (c) the ratio of A/C_i-based T_u ($T_{u,i}$) to A/C_c-based T_u ($T_{u,c}$). Results are based on measured A/C_i curves.

separate analyses within different plant functional types (e.g. herbs versus trees) and climates (e.g. tropical versus temperate regions) did not qualitatively change our findings regarding parameter relationships. Figure 3 shows the ratios of the estimated A/C_i-based to A/C_c-based parameters as a function of mesophyll conductance. The A/C_i-based parameters are smaller than the A/C_c-based values, showing that omission of g_m leads to underestimation of true parameters. The degree of underestimation depends on the magnitude of g_m and can be up to 75, 60 and 40% for V_{cmax}, J_{max}, and T_u, respectively. As mesophyll conductance increases, the two sets of parameters tend to converge, an expected consequence of the A/C_i-based estimation assuming an infinite mesophyll conductance. The $V_{cmax,i}$ (Fig. 3a) appears to be the most sensitive parameter to the variation of mesophyll conductance, and $J_{max,i}$ (Fig. 3b) and $T_{u,i}$ (Fig. 3c) have intermediate and lowest sensitivity, respectively.

Because of variable parameter sensitivities to mesophyll conductance, the relationships among $V_{cmax,i}$, $J_{max,i}$ and $T_{u,i}$ differ from those among $V_{cmax,c}$, $J_{max,c}$ and $T_{u,c}$. Figure 4 shows these functional relationships obtained from A/C_i-based (Fig. 4a,c,e) and from A/C_c-based estimations (Fig. 4b,d,f). The ratios of $J_{max,i}$ to $V_{cmax,i}$ (1.6845), $T_{u,i}$ to $V_{cmax,i}$ (0.1247) and $T_{u,i}$ to $J_{max,i}$ (0.0744) are all larger than their counterparts from the A/C_c-based parameters ($J_{max,c}/V_{cmax,c}$ = 1.1246, $T_{u,c}/V_{cmax,c}$ = 0.0776 and $T_{u,c}/J_{max,c}$ = 0.0697). Moreover, the relationships among the A/C_i-based parameters are tighter than those among the A/C_c-based parameters, as indicated by the corresponding R^2 values. As shown later, the same pattern is obtained with simulated A/C_i curves, confirming that the greater scatter is due to actual variability, not a result of the need to fit for one more unknown parameter with measurements that may contain noise. These results are important as they suggest that the actual coupling among the key parameters V_{cmax}, J_{max} and T_u of the photosynthetic machineries, which has been exploited widely both in experimental and modelling studies, may not be as strong as previously thought.

Among the three photosynthetic parameters, the relationship between T_u and J_{max} is tighter than that between J_{max} and V_{cmax}, which in turn is tighter than that between T_u and V_{cmax}. The same order of goodness-of-fit relationship is preserved regardless whether g_m is assumed infinite (Fig. 4a,c,e) or estimated explicitly (Fig. 4b,d,f).

Figures 3 and 4 indicate that a simple linear function is not adequate to convert the A/C_i-based parameters to the corresponding A/C_c-based values, confirming the suggestion by Niinemets *et al.* (2009c). To achieve more accurate conversion, we used a non-linear model with both the A/C_i-based parameters and g_m as inputs:

$$y = x\exp\left(a\frac{x^c}{g_m^b + d}\right) \quad (4)$$

In the equation shown above, (x, y) represents the pairs of ($V_{cmax,i}$, $V_{cmax,c}$), ($J_{max,i}$, $J_{max,c}$), and ($T_{u,i}$, $T_{u,c}$) and a, b, c, and d are empirical constants that differ among these pairs. The values of a, b, c and d are given in Table 1. Figure 5 demonstrates that this non-linear function performs well in quantifying the relationships between the apparent and corresponding true parameters. Although the empirical constants a, b, c, and d are determined with measurements, the conversion function Eqn 4 with these coefficients also fits the simulated data very well (Supporting Information Fig. S1). As the simulated data were not used in the estimation of a, b, c, and d and were completely independent of the measurements, the good fit of the simulated data indicates that the conversion function Eqn 4 is not limited to the data used in the estimation of its coefficients and rather, it is robust and general.

Equation 4 was found through trials and failures. But more importantly, it has the correct asymptotic behavior when g_m is infinitely large, that is the A/C_i-based parameters converge to the A/C_c-based parameters ($x = y$) and is consistent with our intuitive thinking about how g_m should affect the estimated

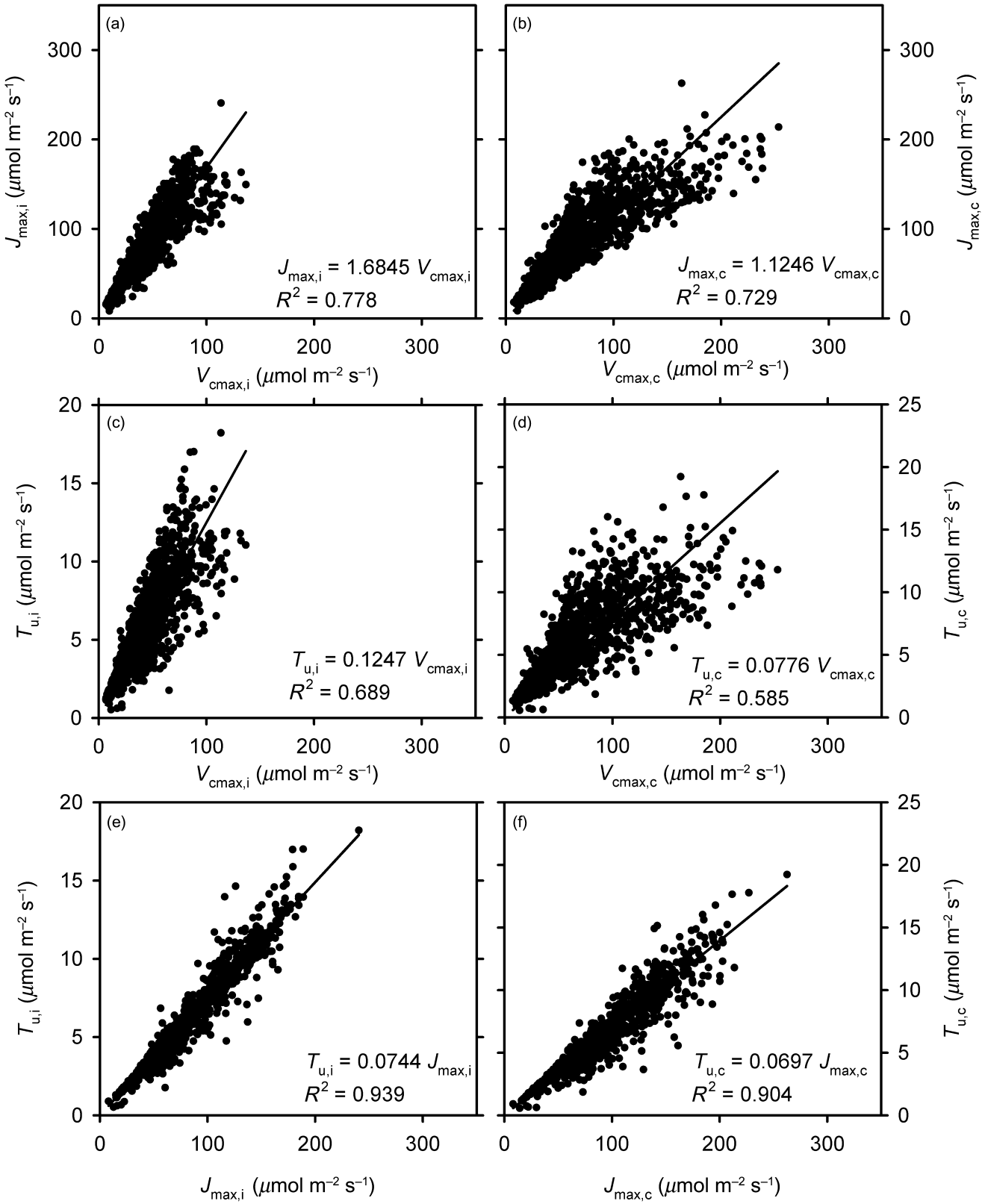

Figure 4. A comparison of the A/C_i-based parameter relationships with the A/C_c-based parameter relationships. The A/C_i-based parameters are estimated by assuming infinite mesophyll conductance while the A/C_c-based parameters are estimated together with mesophyll conductance. (a, c, e) The relationships among the A/C_i-based V_{cmax} ($V_{cmax,i}$), J_{max} ($J_{max,i}$) and T_u ($T_{u,i}$); (b, d, f) the relationships among the A/C_c-based V_{cmax} ($V_{cmax,c}$), J_{max} ($J_{max,c}$) and T_u ($T_{u,c}$). Results are based on measured A/C_i curves.

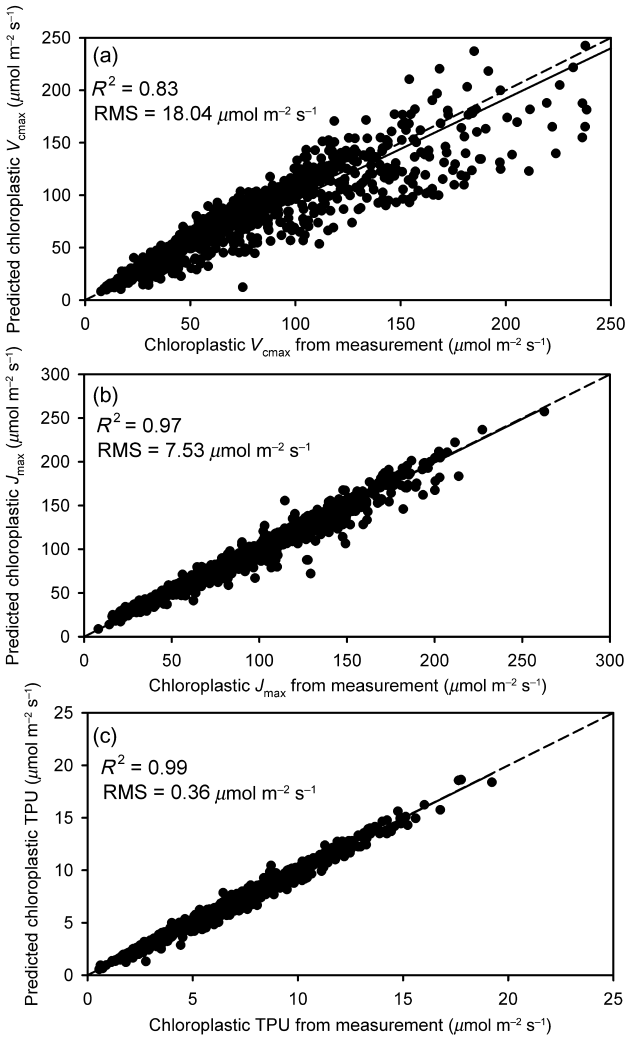

Figure 5. The goodness of fit for Eqn 4, which calculates the A/C_c-based parameters from the A/C_i-based parameters and mesophyll conductance. The A/C_i-based parameters are estimated by assuming infinite mesophyll conductance while the A/C_c-based parameters are estimated together with mesophyll conductance. The values calculated from Eqn 4 are in the y axis while the values estimated from curve fitting are in the x axis. Results are based on measured A/C_i curves.

photosynthetic parameters, that is when g_m decreases and thus the diffusion of CO_2 inside the leaf is retarded by greater resistance, the ratio of y/x increases, indicating the A/C_i-based parameters (x) increasingly underestimate the A/C_c-based parameters (y). In the following section, we demonstrate that these findings still hold for parameters obtained from simulated A/C_i curves.

Results based on simulated *A/C*$_i$ curves

The analysis of simulated A/C_i curves demonstrates that the apparent, A/C_i-based parameters generally underestimate their corresponding true values and this underestimation is more pronounced at lower g_m values, consistent with results from measured A/C_i curves (comparing Fig. 6b,d,f with Fig. 3a,b,c). Several additional patterns also emerge. First, for a given value of true parameter $V_{cmax,c}$, the A/C_i-based $V_{cmax,i}$ increases with g_m and asymptotically approaches its true value as g_m increases (Fig. 6a). Second, the covariation of $V_{cmax,i}$ and g_m (the slope of the $V_{cmax,i} - g_m$ curve for a given $V_{cmax,c}$) is steeper at lower g_m values, but flattens as g_m increases (Fig. 6a). Third, the magnitude of the true parameter $V_{cmax,c}$ affects the relationship between g_m and the apparent, A/C_i-based $V_{cmax,i}$, with a larger $V_{cmax,c}$ resulting in a greater deviation of $V_{cmax,i}/V_{cmax,c}$ ratio from unity (Fig. 6b), suggesting that the assumption of an infinite g_m disproportionately biases the estimation of plants with high photosynthetic capacities.

Similar characteristics are found for the apparent parameters $J_{max,i}$ and $T_{u,i}$, but again, with reduced sensitivities (Fig. 6c–f). Note the missing points in Fig. 6c–f at low g_m values. Without explicit consideration of g_m, A/C_i curve analyses would not be able to properly identify the three limitation states in a set of points. When g_m values are quite small, even the very presence of RuBP regeneration and TPU limitation states in the dataset may not be identified, explaining the missing points in Fig. 6c–f.

Figure 7 emphasizes different aspects from Fig. 6. The underestimated $V_{cmax,i}$ increasingly deviates from $V_{cmax,c}$ as $V_{cmax,c}$ increases and as g_m decreases (Fig. 7a). The ratio of $V_{cmax,i}$ to $V_{cmax,c}$ decreases with $V_{cmax,c}$, with a faster rate at low $V_{cmax,c}$ and g_m values than at high $V_{cmax,c}$ and g_m values (Fig. 7b). Again, Fig. 7 demonstrates that the effects of mesophyll conductance on $J_{max,i}$ and $T_{u,i}$ are broadly similar to those on $V_{cmax,i}$, but with reduced sensitivities (Fig. 7c–f). The decreasing sensitivity to mesophyll conductance from $V_{cmax,i}$ to $J_{max,i}$ to $T_{u,i}$ is revealed by an increasingly tighter linear relationship between the apparent and true parameters (from Fig. 7a to c to e) and by having ratios increasingly close to unity (from Fig. 7b to d to e).

Consistent with patterns shown in Fig. 4 from measured A/C_i curves, Fig. 8 demonstrates that the relationships among V_{cmax}, J_{max} and T_u are altered in the absence of explicit consideration of g_m. The relationships among $V_{cmax,i}$, $J_{max,i}$ and $T_{u,i}$ are tighter than those among $V_{cmax,c}$, $J_{max,c}$ and $T_{u,c}$. The higher goodness-of-fit is essentially an artefact, a consequence of the decreased freedom of variation in the estimated $V_{cmax,i}$, $J_{max,i}$ and $T_{u,i}$ when a finite g_m is assumed to be infinitely large. We can reach this conclusion even though there is one additional parameter to estimate with the consideration of g_m, because measurement uncertainties are not present in the simulated datasets and therefore cannot explain the change in the goodness-of-it with the addition of one more parameter to estimate. The ratio of $J_{max,i}$ to $V_{cmax,i}$ (1.69), is larger than the ratio of $J_{max,c}$ to $V_{cmax,c}$ (1.30). Similarly, the ratios of $T_{u,i}$ to $V_{cmax,i}$ (0.11, Fig. 8c) and to $J_{max,i}$ (0.07, Fig. 8e) are larger than the corresponding ratios of $T_{u,c}$ to $V_{cmax,c}$ (0.08, Fig. 8d) and to $J_{max,c}$ (0.06, Fig. 8f). The decreases in these ratios from the A/C_i-based parameters to the A/C_c-based parameters are a result of reduced underestimation and sensitivity to mesophyll conductance from $V_{cmax,i}$ to $J_{max,i}$ to $T_{u,i}$. These ratios are very close to their counterparts obtained with measured A/C_i

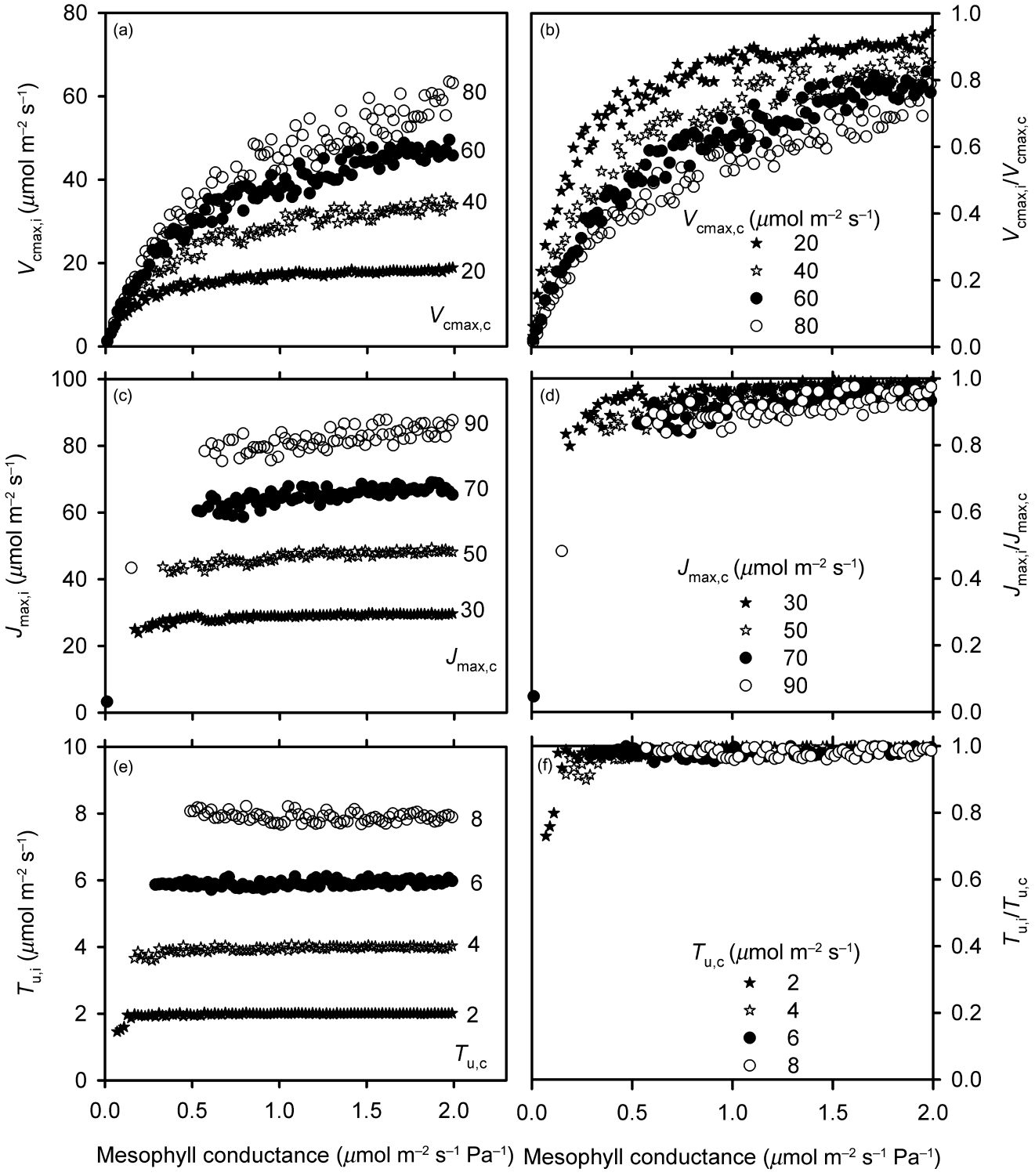

Figure 6. The relationships between the A/C_i-based parameters and mesophyll conductance for a given set of values of A/C_c-based parameters. The A/C_i-based parameters are estimated by assuming infinite mesophyll conductance while the A/C_c-based parameters are estimated together with mesophyll conductance. (a, c, e) the A/C_i-based V_{cmax} ($V_{cmax,i}$), J_{max} ($J_{max,i}$) and T_u ($T_{u,i}$) as a function of mesophyll conductance for a given set of values of A/C_c-based V_{cmax} ($V_{cmax,c}$), J_{max} ($J_{max,c}$) and T_u ($T_{u,c}$), respectively; (b, d, f) the ratios of A/C_i-based to A/C_c-based parameters as a function of mesophyll conductance for a given set of values of A/C_c-based parameters. Results are based on simulated A/C_i curves.

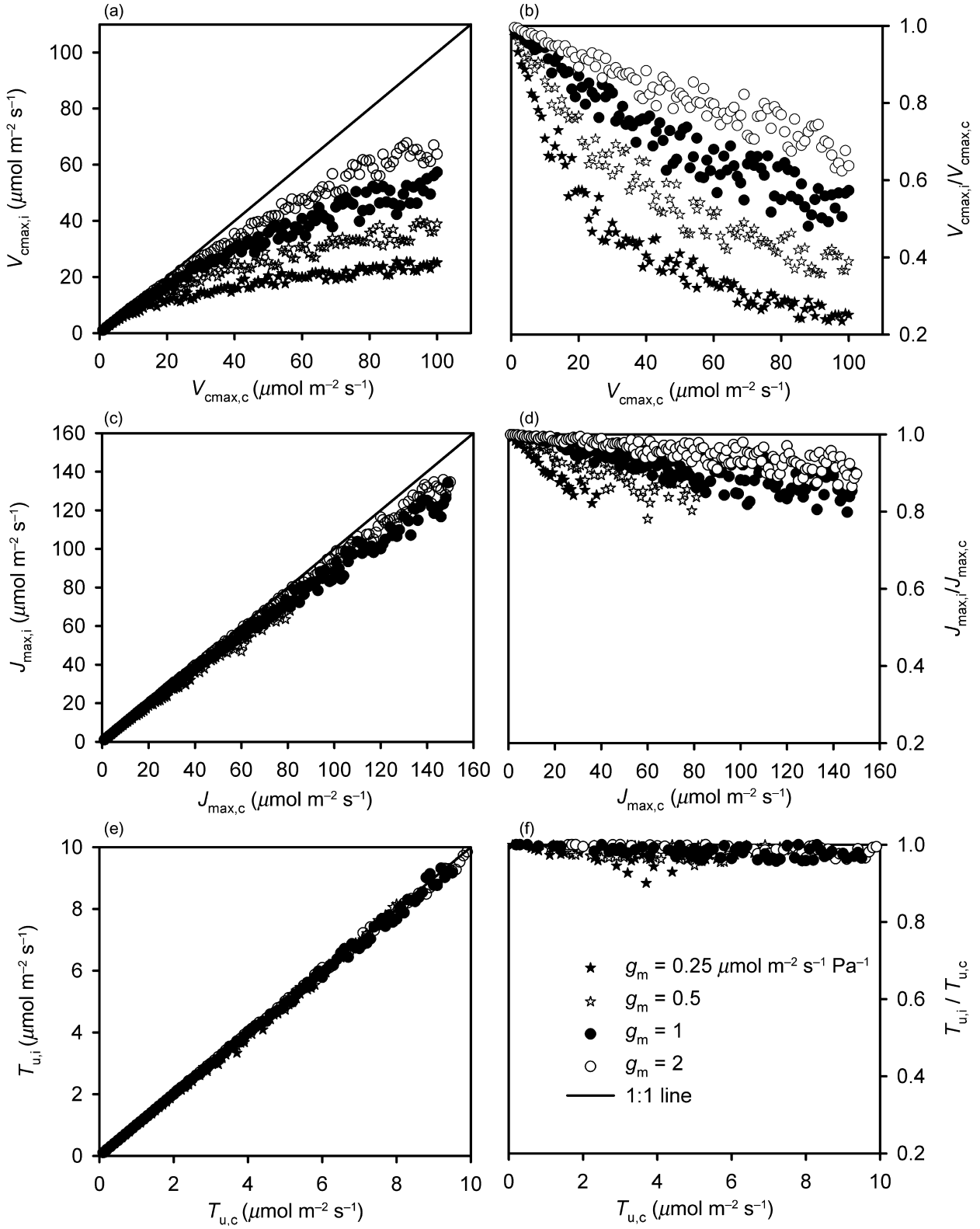

Figure 7. The relationships between the A/C_i-based and A/C_c-based parameters for a given set of values of mesophyll conductance. The A/C_i-based parameters are estimated by assuming infinite mesophyll conductance while the A/C_c-based parameters are estimated together with mesophyll conductance. (a, c, e) the A/C_i-based V_{cmax} ($V_{cmax,i}$), J_{max} ($J_{max,i}$) and T_u ($T_{u,i}$) as a function of A/C_c-based V_{cmax} ($V_{cmax,c}$, a), J_{max} ($J_{max,c}$, c) and T_u ($T_{u,c}$, e), respectively, for a given set of values of mesophyll conductance; (b, d, f) the ratios of A/C_i-based to A/C_c-based parameters as a function of A/C_c-based parameters for a given set of values of mesophyll conductance. Results are based on simulated A/C_i curves.

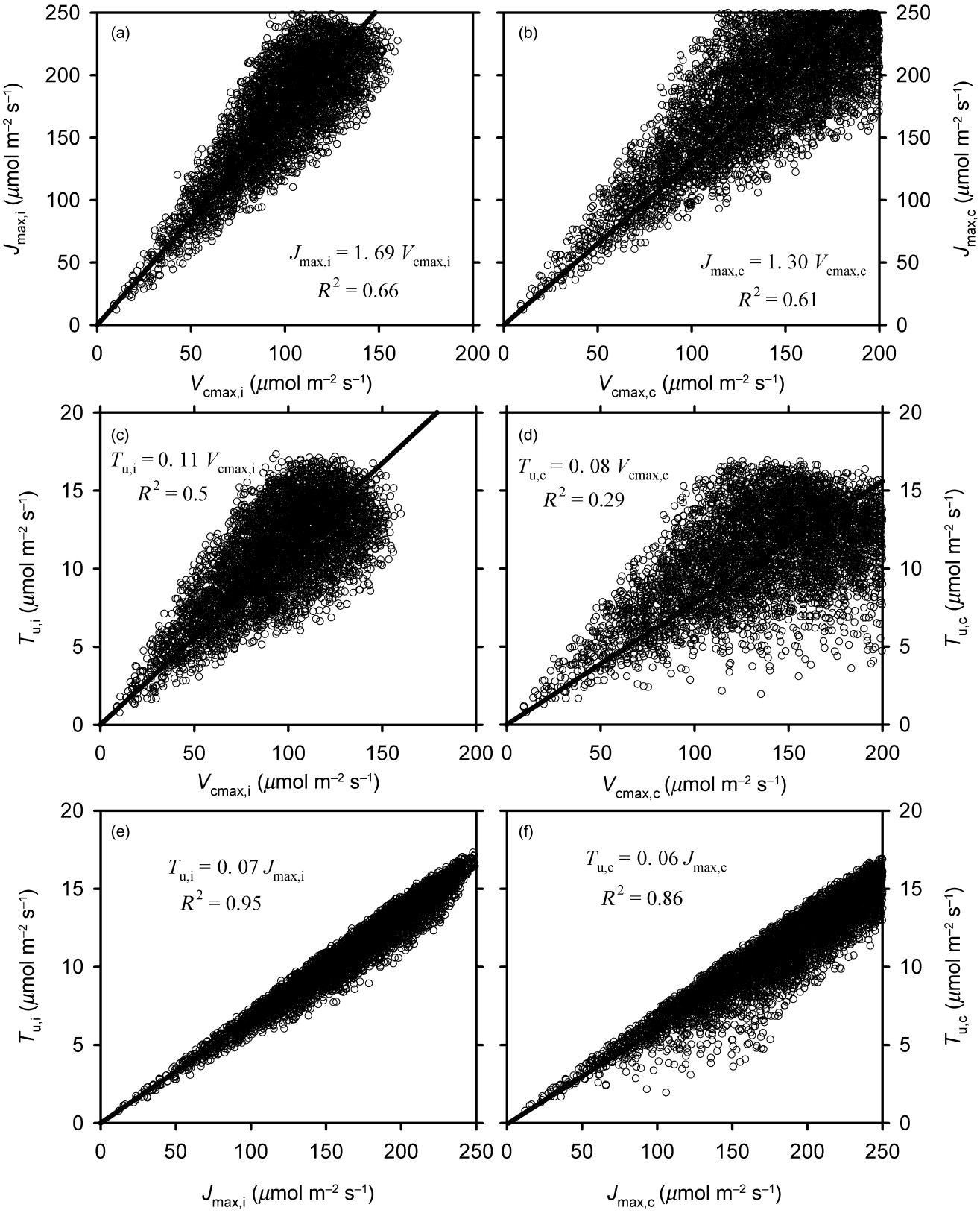

Figure 8. Same as Figure 4 but for simulated A/C_i curves.

curves (comparing the corresponding slope values listed in Figs 4 & 8).

Also consistent with results based on measured A/C_i curves is the order of goodness-of-fit of the relationships among V_{cmax}, J_{max} and T_u. T_u is more tightly related to J_{max} than to V_{cmax} while the goodness-of-fit between V_{cmax} and J_{max} lies between that of T_u and J_{max} and that of T_u and V_{cmax}. Whether g_m is assumed infinite (Fig. 8a,c,e) or estimated (Fig. 8b,d,f) does not affect this order.

DISCUSSION

Our synthesis of worldwide datasets of A/C_i curves demonstrates that the assumption of infinite g_m has asymmetrical impacts on the estimates of V_{cmax}, J_{max} and T_u from leaf gas exchange measurements and can therefore distort the true relationships among these parameters. Our finding has implications not only for process-based studies, but also for large-scale modelling. Global carbon cycle models commonly rely on the relationships among V_{cmax}, J_{max} and T_u for parameterizations of carbon assimilation and for establishing the impact of nutrient availability on photosynthesis (Kattge *et al*. 2009; Bonan *et al*. 2011). These relationships have also been used as measures of balance among different limiting processes of the photosynthetic machineries in evaluating the response of leaf photosynthesis to changes in CO_2 concentration, temperature, and nutrient conditions (Hikosaka 2005; Onoda *et al*. 2005a,b). Our findings suggest that mesophyll conductance may complicate the interpretation of photosynthetic parameter relationships in the context of the operation of photosynthetic machineries and current parameterizations of photosynthetic processes in carbon cycle models may need to be re-evaluated with explicit representation of g_m.

Our study provides direct avenues for improving the representation of photosynthesis in large-scale carbon cycle models by quantifying the role of g_m in shaping key model parameters and regulating photosynthesis. Current global carbon cycle models rely on C_i and employ photosynthetic parameters estimated under the assumption of an infinite g_m. These models ignore the drawdown of CO_2 partial pressures from the substomatal cavity to chloroplast and therefore overestimate the CO_2 concentrations at which the photosynthetic machineries are actually operating in the current atmosphere. Consequently it may be difficult for them to adequately simulate the responsiveness of terrestrial carbon cycles to rising atmospheric CO_2 concentrations. Our conversion function Eqn 4 could be applied to transform the apparent, A/C_i-based parameters, which have been widely reported and applied in the literature, to their corresponding true values for use in mesophyll conductance-represented global carbon cycle models.

Several previous studies based on the variable *J* method have reported that g_m rapidly decreases with increasing C_i and with decreasing irradiance (Flexas *et al*. 2007; Hassiotou *et al*. 2009; Vrábl *et al*. 2009). A few studies with the online carbon isotope discrimination method have also indicated a small dependence of g_m on C_i (Tazoe *et al*. 2011; Douthe *et al*. 2012). However, Gu & Sun (2013) showed that both the variable *J* method and the online carbon isotope discrimination method are sensitive to errors in input parameters and this sensitivity can explain the reported patterns of g_m with C_i and irradiance. Given the real possibility that the previously reported relationship between g_m and C_i and irradiance may be a methodological artefact, this issue is not addressed in this study.

Different temperature response functions and coefficients are available for describing the dependence of photosynthetic parameters on temperature. The functions used in this study are those commonly used by plant physiologists and biochemists (Sharkey *et al*. 2007). Most temperature response functions are fairly similar when temperature is around 25 °C and only deviate from each other when temperature is too low and too high (e.g. see Medlyn *et al*. 2002). All A/C_i curve measurements used in this analysis were obtained under temperature control and no measurements under extreme low or high temperatures were used (the average temperature in our study is 26±5 °C). Thus we do not believe using different temperature response functions will fundamentally change the findings of this study.

The g_m values estimated from our measured A/C_i curves were overwhelmingly within the range of 0.1–10.0 μmol m^{-2} s^{-1} Pa^{-1}. However, the entire range of variation in estimated g_m covers several orders of magnitude (Fig. 3). We do not have enough information to explain such a large range. But we cannot completely rule out the potential impacts of simplifying assumptions in the A/C_i curve analyses. More complicated models and parameters could be introduced to relax these assumptions (Tholen & Zhu 2011; Tholen *et al*. 2012). However, their application may be limited by the fact that the FvCB model is already over-parameterized with respect to typical leaf gas exchange measurements (Gu *et al*. 2010). It is also possible that measurement uncertainties and lack of constraining power in A/C_i curves can cause outliers in estimated g_m. Nevertheless it is reassuring that the results from measured and simulated A/C_i curves are consistent with each other, suggesting that any imperfection in the estimation of g_m likely does not qualitatively affect the findings reported here.

Several methods of mesophyll conductance estimation are now available (Evans *et al*. 1986; Harley *et al*. 1992; Ethier & Livingston 2004; Gu *et al*. 2010) and all are indirect and have strengths and weaknesses (Warren 2006; Pons *et al*. 2009; Gu & Sun 2013). There is a need for a community-wide effort to compare different methods and establish common protocols. Research and technology development for more direct methods of mesophyll conductance estimation is also needed (Sharkey 2012).

CONCLUSION

Mesophyll conductance asymmetrically affects key photosynthetic parameters and their relationships estimated from leaf gas exchange measurements. An assumption of infinite mesophyll conductance leads to underestimation of the maximum carboxylation rate V_{cmax}, maximum electron transport rate J_{max} and triose phosphate utilization rate T_u. The underestimation is more pronounced at lower mesophyll

conductance and at higher photosynthetic capacities. V_{cmax} is the most sensitive parameter to the variation of mesophyll conductance, T_u the least and J_{max} the intermediate. The infinite mesophyll conductance assumption results in overestimation of the ratios of J_{max} to V_{cmax}, T_u to V_{cmax}, and T_u to J_{max}. It also produces artificially close relationships among these parameters. Regardless whether mesophyll conductance is assumed infinite or estimated explicitly, the relationship between T_u and J_{max} is tighter than that between J_{max} and V_{cmax}, which in turn is tighter than that between T_u and V_{cmax}. Finally, a non-linear function can be used to convert the parameters estimated under an assumption of infinite mesophyll conductance to proper values if an estimated mesophyll conductance is available as input.

ACKNOWLEDGMENTS

We thank Dr. Tom Sharkey and two anonymous reviewers for providing insightful suggestions that led to substantial improvements of the paper. This study was carried out at multiple institutions. The support for research at UT – Austin came from the Department of Energy (DE-FG02-01ER63198). The support for research at ORNL came from the U.S. Department of Energy, Office of Science, Biological and Environmental Research Program, Climate and Environmental Sciences Division. The ORNL's LDRD programme also partially supported the research. ORNL is managed by UT-Battelle, LLC, for the U.S. Department of Energy under contract DE-AC05-00OR22725. U.S. Department of Energy support for the University of Missouri (Grant DE-FG02-03ER63683) is gratefully acknowledged.

REFERENCES

Bonan G.B., Lawrence P.J., Oleson K.W., Levis S., Jung M., Reichstein M., . . . Swenson S.C. (2011) Improving canopy processes in the Community Land Model version 4 (CLM4) using global flux fields empirically inferred from FLUXNET data. *Journal of Geophysical Research* **116,** G02014.

Busch F.A., Sage T.L., Cousins A.B. & Sage R.F. (2013) C_3 plants enhance rates of photosynthesis by reassimilating photorespired and respired CO_2. *Plant, Cell & Environment* **36,** 200–212.

Chazen O. & Neumann P.M. (1994) Hydraulic signals from the roots and rapid cell-wall hardening in growing maize (*Zea mays* L.) leaves are primary responses to polyethylene glycol-induced water deficits. *Plant Physiology* **104,** 1385–1392.

Douthe C., Dreyer E., Brendel O. & Warren C.R. (2012) Is mesophyll conductance to CO_2 in leaves of three Eucalyptus species sensitive to short-term changes of irradiance under ambient as well as low O_2? *Functional Plant Biology* **39,** 435–448.

Dubois J.-J.B., Fiscus E.L., Booker F.L., Flowers M.D. & Reid C.D. (2007) Optimizing the statistical estimation of the parameters of the Farquhar–von Caemmerer–Berry model of photosynthesis. *New Phytologist* **176,** 402–414.

Ellsworth D.S., Reich P.B., Naumburg E.S., Koch G.W., Kubiske M.E. & Smith S.D. (2004) Photosynthesis, carboxylation and leaf nitrogen responses of 16 species to elevated pCO2 across four free-air CO2 enrichment experiments in forest, grassland and desert. *Global Change Biology* **10,** 2121–2138.

Ethier G.J. & Livingston N.J. (2004) On the need to incorporate sensitivity to CO2 transfer conductance into the Farquhar–von Caemmerer–Berry leaf photosynthesis model. *Plant, Cell & Environment* **27,** 137–153.

Ethier G.J., Livingston N.J., Harrison D.L., Black T.A. & Moran J.A. (2006) Low stomatal and internal conductance to CO2 versus Rubisco deactivation as determinants of the photosynthetic decline of ageing evergreen leaves. *Plant, Cell & Environment* **29,** 2168–2184.

Evans J.R., Sharkey T.D., Berry J.A. & Farquhar G.D. (1986) Carbon isotope discrimination measured concurrently with gas-exchange to investigate CO2 diffusion in leaves of higher-plants. *Australian Journal of Plant Physiology* **13,** 281–292.

Farquhar G.D. & Von Caemmerer S. (1982) Modelling of photosynthetic responses to environmental conditions. In *Physiological Plant Ecology. II. Encyclopedia of Plant Physiology* (New Series) (eds O. Lange, P. Nobel, C. Osmond & H. Ziegler), pp. 550–587. Springer Verlag, Heidelberg.

Farquhar G.D., Von Caemmerer S. & Berry J.A. (1980) A biochemical-model of photosynthetic Co2 assimilation in leaves of C-3 species. *Planta* **149,** 78–90.

Flexas J., Diaz-Espejo A., Galmes J., Kaldenhoff R., Medrano H. & Ribas-Carbo M. (2007) Rapid variations of mesophyll conductance in response to changes in CO_2 concentration around leaves. *Plant, Cell & Environment* **30,** 1284–1298.

Flexas J., Ribas-Carbó M., Diaz-Espejo A., Galmés J. & Medrano H. (2008) Mesophyll conductance to CO2: current knowledge and future prospects. *Plant, Cell & Environment* **31,** 602–621.

Gu L. & Sun Y. (2013) Artifactual responses of mesophyll conductance to CO_2 and irradiance estimated with the variable J and online isotope discrimination methods. *Plant, Cell & Environment* (in press).

Gu L., Pallardy S.G., Tu K., Law B.E. & Wullschleger S.D. (2010) Reliable estimation of biochemical parameters from C3 leaf photosynthesis-intercellular carbon dioxide response curves. *Plant, Cell & Environment* **33,** 1852–1874.

Han Q., Iio A., Naramoto M. & Kakubari Y. (2010) Response of internal conductance to soil drought in sun and shade leaves of adult *Fagus crenata*. *Acta Silvatica & Lignaria Hungarica* **6,** 123–134.

Hanba Y.T., Kogami H. & Terashima I. (2002) The effect of growth irradiance on leaf anatomy and photosynthesis in Acer species differing in light demand. *Plant, Cell & Environment* **25,** 1021–1030.

Harley P.C., Loreto F., Dimarco G. & Sharkey T.D. (1992) Theoretical considerations when estimating the mesophyll conductance to Co2 flux by analysis of the response of photosynthesis to Co2. *Plant Physiology* **98,** 1429–1436.

Hassiotou F., Ludwig M., Renton M., Veneklaas E.J. & Evans J.R. (2009) Influence of leaf dry mass per area, CO_2, and irradiance on mesophyll conductance in sclerophylls. *Journal of Experimental Botany* **60,** 2303–2314.

Hikosaka K. (2005) Nitrogen partitioning in the photosynthetic apparatus of *Plantago asiatica* leaves grown under different temperature and light conditions: similarities and differences between temperature and light acclimation. *Plant and Cell Physiology* **46,** 1283–1290.

Kattge J., Knorr W., Raddatz T. & Wirth C. (2009) Quantifying photosynthetic capacity and its relationship to leaf nitrogen content for global-scale terrestrial biosphere models. *Global Change Biology* **15,** 976–991.

Laisk A., Eichelmann H., Oja V., Rasulov B., Padu E., Bichele I., . . . Kull O. (2005) Adjustment of leaf photosynthesis to shade in a natural canopy: rate parameters. *Plant, Cell & Environment* **28,** 375–388.

Long S.P. & Bernacchi C.J. (2003) Gas exchange measurements, what can they tell us about the underlying limitations to photosynthesis? Procedures and sources of error. *Journal of Experimental Botany* **54,** 2393–2401.

Long S.P., Farage P.K. & Garcia R.L. (1996) Measurement of leaf and canopy photosynthetic CO2 exchange in the field 1. *Journal of Experimental Botany* **47,** 1629–1642.

Manter D.K. & Kerrigan J. (2004) A/Ci curve analysis across a range of woody plant species: influence of regression analysis parameters and mesophyll conductance. *Journal of Experimental Botany* **55,** 2581–2588.

Medlyn B.E., Dreyer E., Ellsworth D., Forstreuter M., Harley P.C., Kirschbaum M.U.F., . . . Loustau D. (2002) Temperature response of parameters of a biochemically-based model of photosynthesis. II. A review of experimental data. *Plant, Cell & Environment* **25,** 1167–1179.

Miao Z., Xu M., Lathrop R.G. & Wang Y. (2009) Comparison of the A-Cc curve fitting methods in determining maximum ribulose 1.5-bisphosphate carboxylase/oxygenase carboxylation rate, potential light saturated electron transport rate and leaf dark respiration. *Plant, Cell & Environment* **32,** 109–122.

Miyazawa S.-I., Yoshimura S., Shinzaki Y., Maeshima M. & Miyake C. (2008) Deactivation of aquaporins decreases internal conductance to CO2 diffusion in tobacco leaves grown under long-term drought. *Functional Plant Biology* **35,** 553–564.

Montpied P., Granier A. & Dreyer E. (2009) Seasonal time-course of gradients of photosynthetic capacity and mesophyll conductance to CO2 across a beech (*Fagus sylvatica* L.) canopy. *Journal of Experimental Botany* **60,** 2407–2418.

Niinemets Ü., Kull O. & Tenhunen J.D. (1998) An analysis of light effects on foliar morphology, physiology, and light interception in temperate deciduous woody species of contrasting shade tolerance. *Tree Physiology* **18,** 681–696.

Niinemets Ü., Ellsworth D.S., Lukjanova A. & Tobias M. (2001) Site fertility and the morphological and photosynthetic acclimation of *Pinus sylvestris* needles to light. *Tree Physiology* **21,** 1231–1244.

Niinemets Ü., Wright I.J. & Evans J.R. (2009a) Leaf mesophyll diffusion conductance in 35 Australian sclerophylls covering a broad range of foliage structural and physiological variation. *Journal of Experimental Botany* **60,** 2433–2449.

Niinemets Ü., Díaz-Espejo A., Flexas J., Galmés J. & Warren C.R. (2009b) Importance of mesophyll diffusion conductance in estimation of plant photosynthesis in the field. *Journal of Experimental Botany* **60,** 2271–2282.

Niinemets Ü., Díaz-Espejo A., Flexas J., Galmés J. & Warren C.R. (2009c) Role of mesophyll diffusion conductance in constraining potential photosynthetic productivity in the field. *Journal of Experimental Botany* **60,** 2249–2270.

Nobel P.S. (2009) *Physicochemical and Enrironmental Plant Physiology* (4th edn), Academic Press, San Diego, CA, p. 582.

Onoda Y., Hikosaka K. & Hirose T. (2005a) Seasonal change in the balance between capacities of RuBP carboxylation and RuBP regeneration affects CO2 response of photosynthesis in Polygonum cuspidatum. *Journal of Experimental Botany* **56,** 755–763.

Onoda Y., Hikosaka K. & Hirose T. (2005b) The balance between RuBP carboxylation and RuBP regeneration: a mechanism underlying the interspecific variation in acclimation of photosynthesis to seasonal change in temperature. *Functional Plant Biology* **32,** 903–910.

Piel C., Frak E., Le Roux X. & Genty B. (2002) Effect of local irradiance on CO(2) transfer conductance of mesophyll in walnut. *Journal of Experimental Botany* **53,** 2423–2430.

Pons T.L., Flexas J., von Caemmerer S., Evans J.R., Genty B., Ribas-Carbo M. & Brugnoli E. (2009) Estimating mesophyll conductance to CO2: methodology, potential errors, and recommendations. *Journal of Experimental Botany* **60,** 2217–2234.

Schwarz P.A., Law B.E., Williams M., Irvine J., Kurpius M. & Moore D. (2004) Climatic versus biotic constraints on carbon and water fluxes in seasonally drought-affected ponderosa pine ecosystems. *Global Biogeochemical Cycles* **18,** GB4007. doi: 10.1029/2004GB002234.

Sharkey T.D. (1985) Photosynthesis in intact leaves of C3 plants: physics, physiology and rate limitations. *The Botanical Review* **51,** 53–105.

Sharkey T.D. (2012) Mesophyll conductance: constraint on carbon acquisition by C3 plants. *Plant, Cell & Environment* **35,** 1881–1883.

Sharkey T.D., Bernacchi C.J., Farquhar G.D. & Singsaas E.L. (2007) Fitting photosynthetic carbon dioxide response curves for C(3) leaves. *Plant, Cell & Environment* **30,** 1035–1040.

Sinclair T.R., Goudriaan J. & De Wit C.T. (1977) Mesophyll resistance and CO2 compensation concentration in leaf photosynthesis models. *Photosynthetica* **11,** 56–65.

Syvertsen J.P., Lloyd J., McConchie C., Kriedemann P.E. & Farquhar G.D. (1995) On the relationship between leaf anatomy and CO_2 diffusion through the mesophyll of hypostomatous leaves. *Plant, Cell & Environment* **18,** 149–157.

Tazoe Y., von Caemmerer S., Estavillo G.M. & Evans J.R. (2011) Using tunable diode laser spectroscopy to measure carbon isotope discrimination and mesophyll conductance to CO2 diffusion dynamically at different CO_2 concentrations. *Plant, Cell & Environment* **34,** 580–591.

Terashima I., Hanba Y.T., Tazoe Y., Vyas P. & Yano S. (2006) Irradiance and phenotype: comparative eco-development of sun and shade leaves in relation to photosynthetic CO2 diffusion. *Journal of Experimental Botany* **57,** 343–354.

Tholen D. & Zhu X.-G. (2011) The mechanistic basis of internal conductance: a theoretical analysis of mesophyll cell photosynthesis and CO2 diffusion. *Plant Physiology* **156,** 90–105.

Tholen D., Ethier G., Genty B., Pepin S. & Zhu X.-G. (2012) Variable mesophyll conductance revisited. Theoretical background and experimental implications. *Plant, Cell & Environment* **35,** 2087–2103.

Von Caemmerer S. (2000) *Biochemical Models of Leaf Photosynthesis, Techniques in Plant Sciences* (2nd edn), p. 165. CSIRO Publishing, Collingwood, Australia.

Von Caemmerer S., Evans J.R., Hudson G.S. & Andrews T.J. (1994) The kinetics of ribulose-1,5-bisphosphate carboxylase/oxygenase *in vivo* inferred from measurements of photosynthesis in leaves of transgenic tobacco. *Planta* **195,** 88–97.

Vrábl D., Vaskova M., Hronkova M., Flexas J. & Santrucek J. (2009) Mesophyll conductance to CO2 transport estimated by two independent methods: effect of variable CO_2 concentration and abscisic acid. *Journal of Experimental Botany* **60,** 2315–2323.

Warren C. (2006) Estimating the internal conductance to CO_2 movement. *Functional Plant Biology* **33,** 431–442.

Warren C.R. (2008) Stand aside stomata, another actor deserves centre stage: the forgotten role of the internal conductance to CO(2) transfer. *Journal of Experimental Botany* **59,** 1475–1487.

Warren C.R., Dreyer E. & Adams M.A. (2003) Photosynthesis-Rubisco relationships in foliage of *Pinus sylvestris* in response to nitrogen supply and the proposed role of Rubisco and amino acids as nitrogen stores. *Trees* **17,** 359–366.

Warren C.R., Low M., Matyssek R. & Tausz M. (2007) Internal conductance to CO2 transfer of adult *Fagus sylvatica*: variation between sun and shade leaves and due to free-air ozone fumigation. *Environmental and Experimental Botany* **59,** 130–138.

Wullschleger S.D. (1993) Biochemical limitations to carbon assimilation in C 3 plants – a retrospective analysis of the A/C i curves from 109 species. *Journal of Experimental Botany* **44,** 907–920.

Yin X., Struik P.C., Romero P., Harbinson J., Evers J.B., Van Der Putten P.E.L. & Vos J. (2009) Using combined measurements of gas exchange and chlorophyll fluorescence to estimate parameters of a biochemical C-3 photosynthesis model: a critical appraisal and a new integrated approach applied to leaves in a wheat (*Triticum aestivum*) canopy. *Plant, Cell & Environment* **32,** 448–464.

Zeng W., Zhou G.S., Jia B.R., Jiang Y.L. & Wang Y. (2010) Comparison of parameters estimated from A/Ci and A/Cc curve analysis. *Photosynthetica* **48,** 323–331.

Received 1 March 2013; received in revised form 27 September 2013; accepted for publication 1 October 2013

SUPPORTING INFORMATION

Additional Supporting Information may be found in the online version of this article at the publisher's web-site:

Figure S1. Comparison of predicted versus original A/C_c-based V_{cmax} (a), J_{max} (b) and TP_U (c) for the simulated A/C_i curve datasets. The prediction was calculated with the conversion function derived from the actual A/C_i curve measurements.

APPENDIX I. LIST OF SPECIES WHOSE A/C_i CURVES ARE USED IN THE STUDY

Species	Location
Abies lasiocarpa	Colorado, USA, 40° 1.97268′ N, 105° 32.78418′ W
Acalypha diversifolia	Gamboa, Republic of Panama, 9° 7.234′ N, 79° 42.108′ W
Acer rubrum	Michigan, USA, 45° 33.583′ N, 84° 42.827′ W
Acer saccharum	Missouri, USA, 38° 44.648′ N, 92° 12.003′ W
Achillea millefolium	North Dakota, USA, 46° 42.925′ N, 99° 26.852′ W
Adenostoma fasciculatum	California, USA, 33° 36.564′ N, 116° 27.036′W
Agropyron repens	North Dakota, USA, 46° 42.925′ N, 99° 26.852′ W
Alchornea costaricensis	Gamboa, Republic of Panama, 9° 7.234′ N, 79° 42.108′ W
Ambrosia psilostachya	North Dakota, USA, 46° 42.925′ N, 99° 26.852′ W
Annona muricata	Viçosa, Brazil, 20° 45.667′ S, 42° 52.162′ W
Antennaria neglecta	North Dakota, USA, 46° 42.925′ N, 99° 26.852′ W
Arabidopsis thaliana	Tennessee, USA, 35° 57.524′ N, 84° 17.252′ W
Arctostaphylos patula	Oregon, USA, 44° 26.232′ N, −121° 34.008′ W
Artemisia absinthium	North Dakota, USA, 46° 42.925′ N, 99° 26.852′ W
Artemisia frigida	North Dakota, USA, 46° 42.925′ N, 99° 26.852′ W
Artemisia ludoviciana	North Dakota, USA, 46° 42.925′ N, 99° 26.852′ W
Artocarpus heterophyllus	Viçosa, Brazil, 20° 45.667′ S, 42° 52.162′ W
Astronium graveolens	Gamboa, Republic of Panama, 9° 7.234′ N, 79° 42.108′ W
Averrhoa carambola	Viçosa, Brazil, 20° 45.667′ S, 42° 52.162′ W
Banksia oblongifolia Cav.	Broken Back Range, NSW Australia, 32° 42.0833′ S, 151° 8.64667′ E
Betula papyrifera	Michigan, USA, 45° 33.583′ N, 84° 42.827′ W
Bixa orellana	Gamboa, Republic of Panama, 9° 7.234′ N, 79° 42.108′ W
Bromus inermis	North Dakota, USA, 46° 42.925′ N, 99° 26.852′ W
Calathea lutea	Gamboa, Republic of Panama, 9° 7.234′ N, 79° 42.108′ W
Calophyllum brasiliense	Gamboa, Republic of Panama, 9° 7.234′ N, 79° 42.108′ W
Calophyllum inophyllum	Gamboa, 9° 7.234′ N, 79° 42.108′ W & Balboa, Ancon, Republic of Panama, 8° 57.728′ N, 79° 32.614′ W
Carex heliophila	North Dakota, USA, 46° 42.925′ N, 99° 26.852′ W
Cariniana sp.	Viçosa, Brazil, 20° 45.667′ S, 42° 52.162′ W
Carya ovata	Missouri, USA, 38° 44.648′ N, 92° 12.003′ W
Casearia commersoniana	Gamboa, Republic of Panama, 9° 7.234′ N, 79° 42.108′ W
Cecropia peltata	Gamboa, Republic of Panama, 9° 7.234′ N, 79° 42.108′ W
Chrysophyllum cainito	Viçosa, Brazil, 20° 45.667′ S, 42° 52.162′ W
Cinnamomum zeylanicum	Viçosa, Brazil, 20° 45.667′ S, 42° 52.162′ W
Cinnamomum triplinerve	Gamboa, Republic of Panama, 9° 7.234′ N, 79° 42.108′ W
Cirsium arvense	North Dakota, USA, 46° 42.925′ N, 99° 26.852′ W
Cirsium flodmanii	North Dakota, USA, 46° 42.925′ N, 99° 26.852′ W
Citharexylum caudatum	Balboa, Ancon, Republic of Panama, 8° 57.728′ N, 79° 32.614′ W
Citrus sp.	Viçosa, Brazil, 20° 45.667′ S, 42° 52.162′ W
Clusia croatii	Gamboa, Republic of Panama, 9° 7.234′ N, 79° 42.108′ W
Clusia peninsulae	Gamboa, Republic of Panama, 9° 7.234′ N, 79° 42.108′ W
Clusia pratensis	Gamboa, Republic of Panama, 9° 7.234′ N, 79° 42.108′ W
Cochlospermum vitifolium	Gamboa, Republic of Panama, 9° 7.234′ N, 79° 42.108′ W
Coffea Arabica	Viçosa, Brazil, 20° 45.667′ S, 42° 52.162′ W
Crescentia cujete	Balboa, Ancon, Republic of Panama, 8° 57.728′ N, 79° 32.614′ W
Cupania scrobiculata	Gamboa, Republic of Panama, 9° 7.234′ N, 79° 42.108′ W
Dalbergia retusa	Gamboa, Republic of Panama, 9° 7.234′ N, 79° 42.108′ W
Doliocarpus dentatus	Gamboa, Republic of Panama, 9° 7.234′ N, 79° 42.108′ W
Doliocarpus olivaceus	Gamboa, 9° 7.234′ N, 79° 42.108′ W & Balboa, Ancon, Republic of Panama, 8° 57.728′ N, 79° 32.614′ W
Eucalyptus dunnii Maiden	Richmond, NSW Australia, 33° 36.671′ S, 150° 44.447′ E
Eucalyptus globulus Labill. *ssp. globulus*	Richmond, NSW Australia, 33° 36.671′ S, 150° 44.447′ E
Eucalyptus melliodora A. Cunn. ex Schauer	Richmond, NSW Australia, 33° 36.671′ S, 150° 44.447′ E
Eucalyptus saligna Sm.	Richmond, NSW Australia, 33° 36.671′ S, 150° 44.447′ E
Eucalyptus sp.	Plantations owned by Fibria Celulose S.A., Aracruz, Brazil, 19° 47.427833′ S, 40°06.6255′ E
Eriobotrya japonica	Viçosa, Brazil, 20° 45.667′ S, 42° 52.162′ W
Eugenia uniflora	Viçosa, Brazil, 20° 45.667′ S, 42° 52.162′ W
Genipa Americana	Viçosa, Brazil, 20° 45.667′ S, 42° 52.162′ W
Geum triflorum	North Dakota, USA, 46° 42.925′ N, 99° 26.852′ W
Glycine max	Tennessee, USA, 35° 57.524′ N, 84° 17.252′ W
Helianthus pauciflorus	North Dakota, USA, 46° 42.925′ N, 99° 26.852′ W
Hieronyma alchorneoides	Gamboa, Republic of Panama, 9° 7.234′ N, 79° 42.108′ W
Hybanthus prunifolius	Gamboa, Republic of Panama, 9° 7.234′ N, 79° 42.108′ W
Hymenaea courbaril	Viçosa, Brazil, 20° 45.667′ S, 42° 52.162′ W
Inga spectabilis	Gamboa, Republic of Panama, 9° 7.234′ N, 79° 42.108′ W
Inga sp.	Viçosa, Brazil, 20° 45.667′ S, 42° 52.162′ W
Jatropha curcas	Gamboa, Republic of Panama, 9° 7.234′ N, 79° 42.108′ W

APPENDIX I. *Continued*

Species	Location
Juniperus virginiana	Missouri, USA, 38° 44.648′ N, 92° 12.003′ W
Litchi chinensis	Viçosa, Brazil, 20° 45.667′ S, 42° 52.162′ W
Luehea seemannii	Gamboa, Republic of Panama, 9° 7.234′ N, 79° 42.108′ W
Malpighia emarginata	Viçosa, Brazil, 20° 45.667′ S, 42° 52.162′ W
Manilkara zapota	Gamboa, Republic of Panama, 9° 7.234′ N, 79° 42.108′ W
Melilotus officinalis	North Dakota, USA, 46° 42.925′ N, 99° 26.852′ W
Merremia sp.	Gamboa, Republic of Panama, 9° 7.234′ N, 79° 42.108′ W
Miconia impetiolaris	Gamboa, Republic of Panama, 9° 7.234′ N, 79° 42.108′ W
Myroxylon balsamum	Gamboa, Republic of Panama, 9° 7.234′ N, 79° 42.108′ W
Nassella viridula	North Dakota, USA, 46° 42.925′ N, 99° 26.852′ W
Ochroma pyramidale	Gamboa, Republic of Panama, 9° 7.234′ N, 79° 42.108′ W
Oligoneuron rigidum	North Dakota, USA, 46° 42.925′ N, 99° 26.852′ W
Omphalea diandra	Balboa, Ancon, Republic of Panama, 8° 57.728′ N, 79° 32.614′ W
Ormosia macrocalyx	Gamboa, Republic of Panama, 9° 7.234′ N, 79° 42.108′ W
Oryza sativa	Viçosa, Brazil, 20° 45.667′ S, 42° 52.162′ W
Oxalis stricta	North Dakota, USA, 46° 42.925′ N, 99° 26.852′ W
Pascopyrum smithii	North Dakota, USA, 46° 42.925′ N, 99° 26.852′ W
Passiflora vitifolia	Gamboa, Republic of Panama, 9° 7.234′ N, 79° 42.108′ W
Peltogyne purpurea	Gamboa, Republic of Panama, 9° 7.234′ N, 79° 42.108′ W
Persoonia levis (Cav.) Domin	Blue Mountains, NSW Australia, 33° 42.466′ S, 150° 32.858′ E
Persea Americana	Viçosa, Brazil, 20° 45.667′ S, 42° 52.162′ W
Philodendron sp.	Gamboa, Republic of Panama, 9° 7.234′ N, 79° 42.108′ W
Phyllostachys humilis	Dublin, Ireland, 53°31.41′ N, 6°15.31′ E
Picea engelmannii	Colorado, USA, 40° 1.97268′ N, 105° 32.78418′ W
Picea mariana	Minnesota, USA, 47° 30.171′ N, 93° 28.97′ W
Pinus contorta	Colorado, USA, 40° 1.97268′ N, 105° 32.78418′ W
Pinus pinaster	Aquitaine, France, 44° 42′ N, 0° 46′ W
Pinus ponderosa	Oregon, USA, 44° 26.232′ N, 121° 34.008′ W
Pinus taeda	North Carolina, USA, 35° 58.692′ N, 79° 5.652′ W
Piper reticulatum	Gamboa, Republic of Panama, 9° 7.234′ N, 79° 42.108′ W
Piper sp.	Gamboa, Republic of Panama, 9° 7.234′ N, 79° 42.108′ W
Pithecellobium mangense	Balboa, Ancon, Republic of Panama, 8° 57.728′ N, 79° 32.614′ W
Platymiscium pinnatum	Gamboa, Republic of Panama, 9° 7.234′ N, 79° 42.108′ W
Poa pratensis	North Dakota, USA, 46° 42.925′ N, 99° 26.852′ W
Populus grandidentata	Michigan, USA, 45° 33.583′ N, 84° 42.827′ W
Populus deltoids	Tennessee, USA, 35° 57.524′ N, 84° 17.252′ W
Psidium guajava	Viçosa, Brazil, 20° 45.667′ S, 42° 52.162′ W
Purshia tridentate	Oregon, USA, 44° 26.232′ N, 121° 34.008′ W
Quercus alba	Missouri, 38° 44.648′ N, 92° 12.003′ W & Tennessee, USA, 35° 57.524′ N, 84° 17.252′ W
Quercus stellata	Missouri, 38° 44.648′ N, 92° 12.003′ W & Tennessee, USA, 35° 57.524′ N, 84° 17.252′ W
Quercus velutina	Missouri, USA, 38° 44.648′ N, 92° 12.003′ W
Quercus rubra	Michigan, 45° 33.583′ N, 84° 42.827′ W & Tennessee, USA, 35° 57.524′ N, 84° 17.252′ W
Rhapis excelsa	Balboa, Ancon, Republic of Panama, 8° 57.728′ N, 79° 32.614′ W
Rosa arkansana	North Dakota, USA, 46° 42.925′ N, 99° 26.852′ W
Schefflera sp.	Balboa, Ancon, Republic of Panama, 8° 57.728′ N, 79° 32.614′ W
Schima superba	Zhejiang, China, 28° 31.83′ N, 118° 33.951′ E
Schinus terebinthifolius	Viçosa, Brazil, 20° 45.667′ S, 42° 52.162′ W
Serjania sp.	Gamboa, Republic of Panama, 9° 7.234′ N, 79° 42.108′ W
Solidago Canadensis	North Dakota, USA, 46° 42.925′ N, 99° 26.852′ W
Solidago missouriensis	North Dakota, USA, 46° 42.925′ N, 99° 26.852′ W
Spondias mombin	Gamboa, Republic of Panama, 9° 7.234′ N, 79° 42.108′ W
Sterculia apetala	Gamboa, Republic of Panama, 9° 7.234′ N, 79° 42.108′ W
Stigmaphyllum sp.	Gamboa, Republic of Panama, 9° 7.234′ N, 79° 42.108′ W
Swietenia macrophylla	Viçosa, Brazil & Balboa, Ancon, Republic of Panama, 8° 57.728′ N, 79° 32.614′ W
Symphyotrichum ericoides	North Dakota, USA, 46° 42.925′ N, 99° 26.852′ W
Symphoricarpos occidentalis	North Dakota, USA, 46° 42.925′ N, 99° 26.852′ W
Syzygium jambos	Viçosa, Brazil, 20° 45.667′ S, 42° 52.162′ W
Tabebuia rosea	Gamboa, 9° 7.234′ N, 79° 42.108′ W & Balboa, Ancon, Republic of Panama, 8° 57.728′ N, 79° 32.614′ W
Taraxacum officinale	North Dakota, USA, 46° 42.925′ N, 99° 26.852′ W
Tectona grandis	Viçosa, Brazil, 20° 45.667′ S, 42° 52.162′ W
Trifolium ambiguum	Minnesota, USA, 44° 43.72′ N, 93° 5.312′ W
Veitchia merrillii	Balboa, Ancon, Republic of Panama, 8° 57.728′ N, 79° 32.614′ W
Vismia bilbergiana	Gamboa, Republic of Panama, 9° 7.234′ N, 79° 42.108′ W
Vitex cooperi	Gamboa, Republic of Panama, 9° 7.234′ N, 79° 42.108′ W
Zuelania Guidonia	Gamboa, Republic of Panama, 9° 7.234′ N, 79° 42.108′ W